Review paper

Electron backscatter diffraction in materials characterization

Dejan Stojakovic[1,2]

[1]*Materion Advanced Materials Group, 42 Mount Ebo Road South, Brewster, NY 10509, USA*
[2]*Materion Corporation, 6070 Parkland Boulevard, Mayfield Heights, OH 44124, USA*

Received 9 November 2011; received in revised form 24 February 2012; accepted 26 February 2012

Abstract

Electron Back-Scatter Diffraction (EBSD) is a powerful technique that captures electron diffraction patterns from crystals, constituents of material. Captured patterns can then be used to determine grain morphology, crystallographic orientation and chemistry of present phases, which provide complete characterization of microstructure and strong correlation to both properties and performance of materials. Key milestones related to technological developments of EBSD technique have been outlined along with possible applications using modern EBSD system. Principles of crystal diffraction with description of crystallographic orientation, orientation determination and phase identification have been described. Image quality, resolution and speed, and system calibration have also been discussed. Sample preparation methods were reviewed and EBSD application in conjunction with other characterization techniques on a variety of materials has been presented for several case studies. In summary, an outlook for EBSD technique was provided.

Keywords*: EBSD, characterization, microstructure, properties*

Contents

I. Introduction

Electron Back-Scatter Diffraction (EBSD) or Electron Back-Scatter Pattern (EBSP) is a powerful technique that captures electron diffraction patterns from crystals, constituents of material. Captured patterns can then be used to determine the crystallographic orientation or texture of materials, which is strongly correlated to both properties and performance of materials. Therefore, the understanding and control of preferred crystallographic orientation is of fundamental importance in material design as well as in material processing. EBSD technique can be

* Corresponding author: tel: +1 845 278 5419
fax: +1 845 279 0922, e-mail: *dejan@drexel.edu*

applied on a variety of materials, such as metals and alloys, minerals, ceramics and semiconductors.

Almost a century ago the first observation of EBSP was reported by Japanese physicist Seishi Kikuchi [1] in which honour the alternative name is Backscatter Kikuchi Diffraction (BKD). Since then considerable work has been done in identifying the crystallographic orientation associated with EBSP. It was not until two decades ago that technique started gaining popularity when Stuart I. Wright [2] in his doctoral dissertation at Yale University in USA, developed a fully automated orientation determination from EBSP, which allowed faster EBSD data acquisition and processing. Automation has allowed EBSD to become a more practical technique and following with subsequent parallel advancement in both hardware and software developments, the EBSD technique gained in accuracy, speed and versatility. Some of the key milestones related to technological developments of EBSD technique are chronologically listed in Table 1.

Microstructure is viewed as the connection between science and technology of materials which provides an important link between properties and performance of materials. Typically, microstructure is expressed mainly in terms of grain size and morphology, however, complete characterization of microstructure requires both crystallographic and chemical information. Back in late 19th century a British scientist Henry Sorby [25] was the first to reveal grain morphology under optical microscope by chemical etching of polished iron and steel samples. It was not until mid 20th century when a French physicist Raimond Castaing [26] developed an electron microprobe elemental analysis that enabled characterization of major, minor and trace phases. The first commercial Scanning Electron Microscope (SEM) became available in 1965 and since then the technology has progressed considerably and today EBSD is well established analytical technique in SEM for microstructural analyses of most crystalline materials. Furthermore, EBSD system can be integrated with both Energy Dispersive Spectroscopy (EDS) and Wavelength Dispersive Spectroscopy (WDS) providing a powerful tool for in depth characterization of microstructure in SEM. Today, EBSD technique is well established in academia and technique is also gaining popularity in the area of industrial research and development. Some possible applications using modern EBSD system are listed in Table 2.

Other techniques capable to provide diffraction information are coarser-scale Kossel diffraction and finer-scale diffraction in Transmission Electron Microscope (TEM). In addition, SEM equipped with Focused Ion Beam (FIB) provides capabilities for additional (third) dimension in characterization of microstructure by means of in-situ serial sectioning of material and reconstruction of EBSD data from two-dimensional (planar) sections into three-dimensional (3D) microstructure. The alternative, non-destructive technique for characterization of microstructure in 3D is synchrotron radiation, which involves the use of high intensity, very short wavelength X-rays (3DXRD).

The introductory chapter is followed by brief description of crystallographic orientation, crystal diffraction, orientation determination, phase identification, image quality, resolution and speed, system calibration, sample preparation, applications on a variety of materials and outlook.

Table 1. Milestones in development of EBSD technique

Year	Milestone	Reference
1928	The discovery of a divergent beam diffraction pattern	[1,3]
1933	Observation of wide angle diffraction pattern	[4]
1937	Study of transmission and backscatter Kikuchi patterns	[5]
1948	Use of dynamic theory of electron diffraction for formation of Kikuchi bands	[6]
1954	Observation of high angle Kikuchi patterns	[7]
1973	Determination of lattice orientation by EBSP, introduction into SEM	[8]
1984	Use of video camera for viewing EBSP	[9]
1986	Orientation mapping by continuous colour coding	[10,11]
1986	Application of EBSP for phase identification	[12,13]
1987	On-line indexing of EBSP	[14]
1989	Use of bands instead of zone axes to identify lattice orientation	[15]
1990	Bands detection by segmenting EBSP into binary images	[16]
1991	First attempt to automatically determine orientation from EBSP	[2,17]
1992	Another attempt to identify bands by use of Burns algorithm	[18]
1992	Use of Hough Transform for band detection – widely used today	[19,20]
1993	Description of the first fully automated EBSD system in SEM	[21]
1997	Invention of confidence index (CI) for correctly indexed data	[22]
1997	First commercial integrated EBSD/EDS system	[23]
2002	Report on the first chemistry assisted phase differentiation during scan	[24]

Table 2. Application areas for EBSD technique in materials characterization

Application	Characterization
Materials development	- texture measurement and mapping - texture evolution and gradients - strain gradient measurement and mapping - grain morphology and grain fragmentation - grain boundary character distribution - phase identification - phase distribution and phase transformation
Process quality and control	- texture control in deformation and annealing processes - heat treating effect on structural changes - heterogeneity of structure in welds - texture gradients in sputtering targets - grain size and texture in microelectronic devices - epitaxial layer in thin films - retained ferrite and austenite measurements in steel
Failure analysis	- texture effect on crack propagation behavior - grain boundary effect on corrosion, fracture and fatigue - grain boundary segregation and precipitation effect on creep - grain boundary sliding - identification of defects

II. Crystallographic orientation

The majority of industrial materials are made up of many crystals (grains), each of which has an ordered structure. These crystals all fit perfectly together to form a solid polycrystalline material. Although the structure within each of these crystals is ordered they are not aligned with the internal structure of the neighbouring grains. This creates a grain boundary, which is an interface between two crystals whose structures are not geometrically aligned. These crystals are said to have different orientations or three dimensional configurations relative to the sample reference frame (Fig. 1a). Orientation of individual crystals (grains) within a polycrystalline sample can be described as the rotation, which transforms the fixed sample's coordinate system into fixed crystal's coordinate system [27]. Usually, sample's coordinate system is defined by rolling (RD), transverse (TD) and normal (ND) orthogonal directions and crystal's coordinate system is defined by Miller indices of cube direction [100], [010] and [001] which are also orthogonal (Fig. 1b).

The orientation of a crystal relative to the sample reference frame can be represented by three rotations, also referred to as Euler angles (φ_1, φ, φ_2). There are multiple conventions for representing these rotations and the most commonly used is the Bunge convention [27]. The Bunge convention rotates the sample reference frame into the crystal frame and the rotation is represented by the three Bunge-Euler angles. The three angles of rotation in the Bunge-Euler convention must be performed in the specific order relative to a specific axis of rotation to transform the sample axes to the crystal axes (Fig. 2). Angle φ_1 is the first angle of rotation and is performed anticlockwise about the ND axis, φ is the second rotation and is performed anticlockwise about the RD' axis, and φ_2 is the final rotation and is performed anticlockwise about the ND' axis. A complete description of texture can be expressed in terms of an orientation distribution function (ODF) plot in a three-dimensional orientation space, also called an Euler space [27]. In Euler space orientations are plotted as a function of three Bunge-Euler angles, actually orientations are shown in sections as a function of two Bunge-Euler angles for a fixed value of a third angle.

In general, the crystallographic orientation of polycrystalline materials is not random, meaning that there

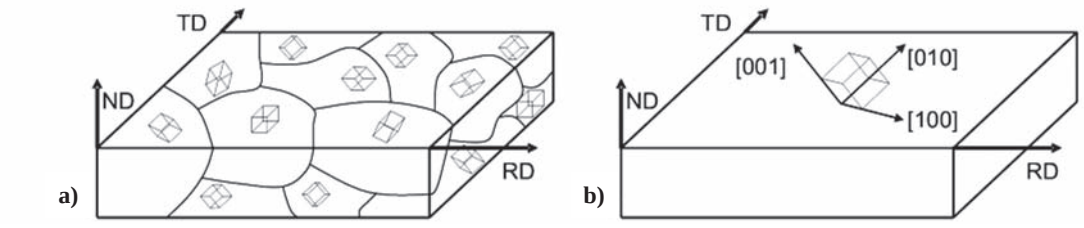

Figure 1. Schematic representation of: a) polycrystalline microstructure depicting the different orientation of the crystals, b) sample reference frame and crystal frame inside the bulk material

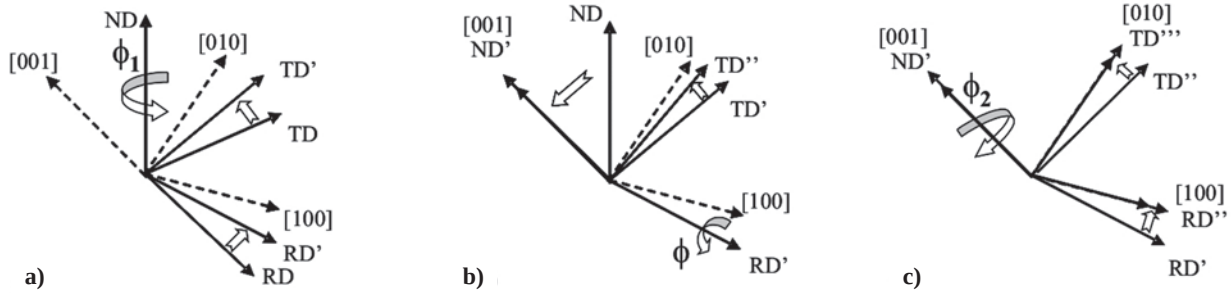

Figure 2. Schematic representation of the Bunge-Euler convention, which rotates the sample reference frame into the crystal reference frame

is a preferred crystallographic orientation of the individual crystals, also known as "texture". The significance of texture lies in the anisotropy of many macroscopic material properties (elastic modulus, strength, toughness, ductility, thermal expansion, electrical conductivity, magnetic permeability and energy of magnetization) [28].

III. Crystal diffraction

EBSD patterns are obtained by focusing electron beam on a crystalline sample. The sample is tilted to approximately 70 degrees with respect to the horizontal (usually done by tilting the SEM stage with sample holder) which allows more electrons to be scattered and to escape towards the detector. The electrons disperse beneath the surface, subsequently diffracting among the crystallographic planes. The diffracted electrons which interfered constructively, expressed by Bragg's Law [29], produce a pattern composed of intersecting bands (Kossel cones). Diffraction angles have small values of 1 or 2 degrees, thus the bands appear as straight lines on the screen. Diffracted patterns are imaged by placing a phosphor screen in front of EBSD camera close to the sample in the SEM chamber (Fig. 3). The phosphor in the screen interacts with diffracted electrons and emits light suitable for camera to record (today's camera is equipped with Charge-Coupled Device (CCD) chip and earlier version was Silicon Intensified Tube (SIT) low light video camera).

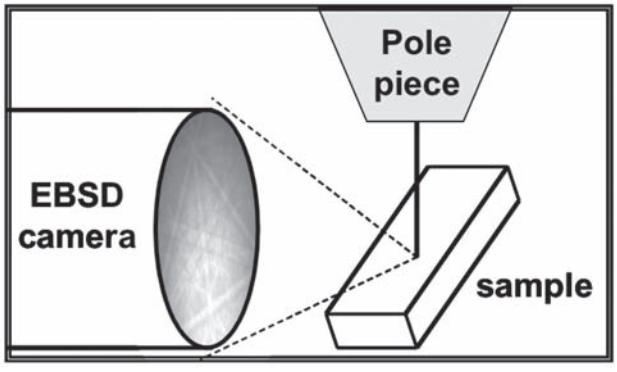

Figure 3. Position of the sample inside the SEM chamber relative to pole piece and phosphorous screen

The bands in the pattern represent the reflecting planes in the diffracting crystal volume. Hence, the geometrical arrangement of bands is a function of the orientation of the diffraction crystal lattice such that: (a) the symmetry of the crystal lattice is reflected in the pattern, (b) the width and the intensity of the bands are directly related to the spacing of atoms in the crystallographic plane and (c) the angles between the bands are directly related to the angles between the crystallographic planes. EBSD patterns from three different materials with different crystal structures are shown in Fig. 4.

IV. Orientation determination

The hearth of EBSD technique is indexing of diffracted patterns (extraction of the bands from the pattern). If the sample produces good diffraction patterns, orientation determination is a three-step process consisting of: (a) Kikuchi band detection, (b) Kikuchi band identification and indexing of pattern, (c) determination of orientation.

In the first step, Kikuchi band detection is carried through Hough Transform [30,31] by converting Kikuchi lines from recorded image into single points in the Hough space. Since the location of the points, instead of lines, can be determined more accurately, the challenge of finding a band in the diffraction pattern is then reduced to finding a peak of high intensity in the Hough space. For every recorded EBSD pattern (e.g. as shown in Fig. 4) a Hough transform is performed (Fig. 5a) and bands are detected (Fig. 5b) automatically.

In the second step, Kikuchi band identification is related to correct identification of particular lattice plane associated with reconstructed Kikuchi band. The width of detected bands is a function of the spacing of diffracting planes (Bragg's law) and is compared to a theoretical list of diffracting lattice planes. Additionally, the angles between bands have to be determined and compared with theoretical values. This is done by comparison with a stored table in the database consisting of all interplanar angles between the low Miller indices [32] planes (hkl) present in the crystal structure, including every individual plane in the family of planes {hkl}. The interplanar angles between three intersecting bands

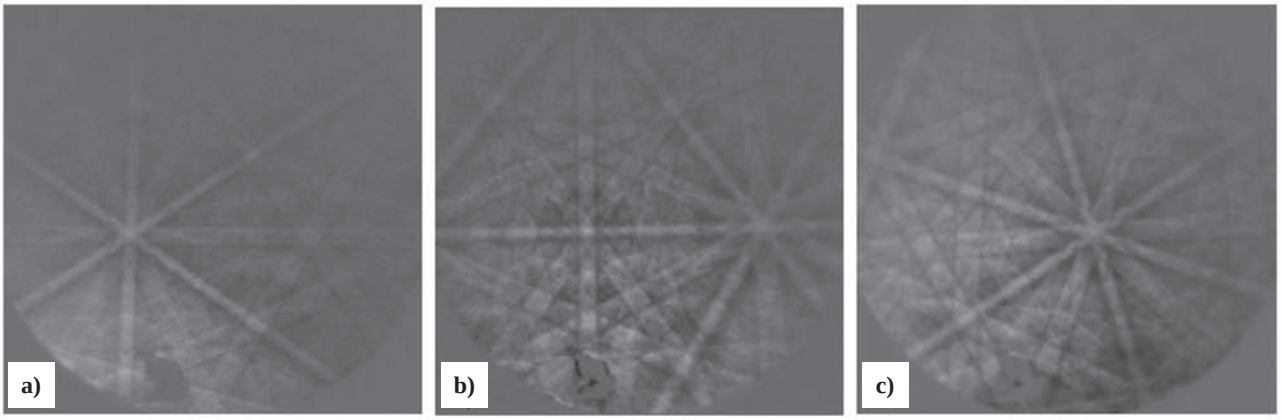

Figure 4. EBSD patterns from: a) commercially pure aluminium with face-center-cubic (FCC) structure, b) electrical steel (Fe-Si alloy) with body-center-cubic (BCC) structure, c) alpha phase titanium with hexagonal-close-packed (HCP) structure

are calculated and compared with the data from table in order to decide their identity within the small tolerance, usually 1 to 2 degrees. Once planes are correctly and consistently identified, zone axes are indexed from cross-product calculations of indexed planes (Fig. 6a). Usually, more than one possible solution can be found for any three bands and parameter called Confidence Index (CI) is used, which is based on a voting scheme. In this procedure, all possible sets of three bands are formed and solution is based on the most probable indexing of the pattern, which is a function of set up tolerance between measured and theoretical interplanar angles. For most structures automated line detection and indexing is reliable and robust. However, for some low symmetry structures it may be necessary for the user to work interactively and to choose the correct solution from the number of indexed options, or to index pattern manually.

In the third step, orientation determination is based on calculation of the orientation of the corresponding crystal lattice with respect to reference frame. Often a sample reference frame is used (as shown in Fig. 1) and sequence of rotations is applied (as shown in Fig. 2) to bring the samples frame into coincidence with the crystal lattice frame. Crystal orientation is than defined by three (φ_1, φ, φ_2) Euler angles (Fig. 6b).

V. Phase identification

EBSD technique in conjunction with the excellent SEM imaging capabilities is also used for identification of crystalline phases in material (employing EBSD in phase identification is a complementary method to TEM). It is important to differentiate between: (a) phase verification and (b) phase identification. In phase verification there is a great deal of certainty of phases presents in material, therefore only several (preselected) choices are searched in crystallographic database. On the other hand in phase identification there is a great deal of uncertainty of phases present and a large database of crystalline compounds would need to be searched for a good match, which would be impractical. To overcome this shortcoming a set of measurable parameters (Fig. 6a) is employed to screen database. Since EBSD patterns contain an ample amount of information about the structure of the crystal (phase) it is used to determine the symmetry of the crystal. Furthermore, EBSD patterns contain Higher Order Laue Zone (HOLZ) rings [33], which are used for high accuracy measurement of lattice spacing and lattice unit cell (an interatomic plane spacing can also be determine from the width of Kikuchi lines, but with less accuracy). In addition, SEM equipped with EDS and, or WDS can provide the qualitative chemistry of the phases present

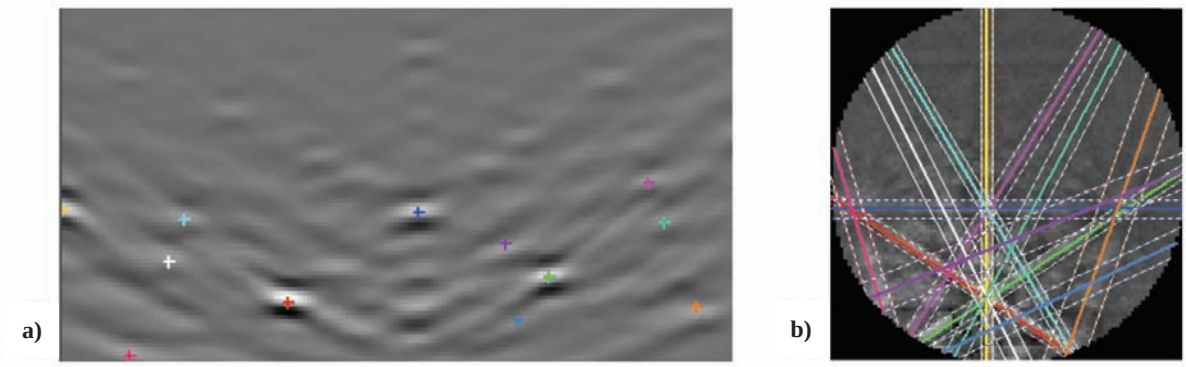

Figure 5. Kikuchi band detection by Hough transform: a) Hough space, b) detected bands reconstructed from Hough space

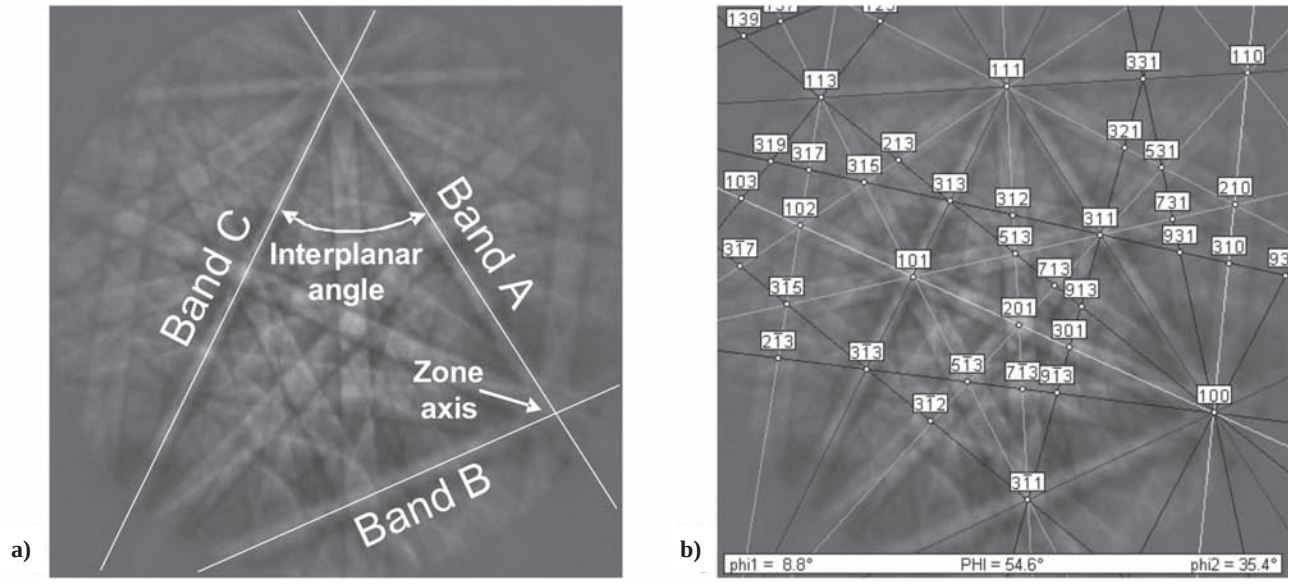

Figure 6. Orientation determination from: a) features in collected pattern and b) indexed pattern

in material and further reduce database search. Phase identification is more of an iterative method, which is also true for orientation determination in crystals with low symmetry.

VI. Image quality

Electrons are diffracted from the near the surface of the sample and image quality can be considered as a parameter related to crystallographic uniformity of characterized volume. Image quality is extracted from the quality of Kikuchi bands (intensity, sharpness, contrast, noise level), which are influenced by topography, grain boundaries, present phases and residual strain in material. Kikuchi bands of high quality have intense Hough peaks and average intensity will be greater than for Kikuchi bands of lower quality. Therefore image quality provides useful complementary information about these features to the indexed crystallographic orientations [34]. In deformed samples the dimensions of crystal lattice are distorted (due to higher dislocation density), which leads to a greater angular distribution (variation) of diffracted crystallographic planes that results in decreased Kikuchi band contrast and blurred Kikuchi band edges [35].

Similar analogy can be made between the different quality of diffracted patterns and the different electron signals (secondary electrons, backscattered electrons, forward scatter electrons) in SEM. Electron signals provide different ways for evaluation of the interaction of the electron beams with sample. Figure 7 shows Forward Scatter Diffraction (FCD) contrast image of deformed sample revealing primary grain boundaries (existing prior to deformation) and deformation bands developed during deformation within grains [36]. FCD imaging can effectively capture variations in topography, orientation and composition. Variations in geometry design between beam, sample and detector, conditions of electron beam and insertion position of EBSD camera can also enhance image contrast.

VII. Resolution and speed

In general two types of resolution are considered, spatial and angular, which are limited by minimum diffracting volume (volume of specimen material that interacts with SEM electron beam) and capability of deconvoluting overlapping EBSD patterns (at the grain or phase boundary where diffraction patterns are emitted from adjacent regions across boundary). The spatial resolution of

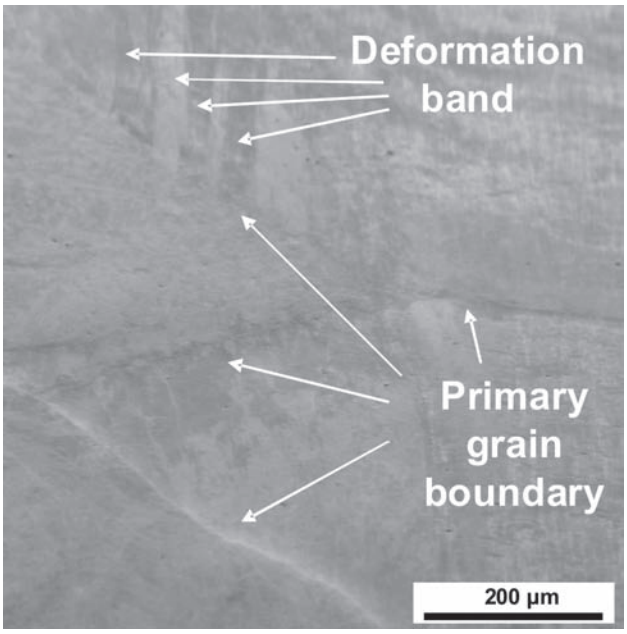

Figure 7. Image quality map of deformed single phase electrical steel (Fe-Si) alloy with noticeable contrasts revealing primary grain boundaries and deformation bands

EBSD measurement is a function of electron probe energy, electron probe diameter and backscattering coefficient (function of atomic number of elements present in material). In the field emission SEM with a Schottky electron beam source using high beam current and small diameter electron beam on material with high atomic number (*Z*) grains as small as 20 nm can be reliably characterized [37]. In the SEM with Tungsten filament the spatial resolution is about three times less than in the field emission SEM. The angular resolution of determining the orientation of the crystal is in the order of 0.5 degree and geometry of the system (SEM pole piece, sample holder and EBSD camera position) must be known.

An impressive progress has been made in data collection speed (data point per second) from the development of automated EBSD when speed of acquisition and indexing was about 10 patterns per second and today, modern systems are capable of achieving a speed of several hundred data points per second, thanks to both software and hardware developments. Another factor that affects speed is mechanical stage scan or digital beam scan as two computer aided sampling modes used in automated EBSD. In the stage controlled scanning mode the sample is translated mechanically under the focused electron beam. The advantage is in achieving large measuring fields, but the stage motion (*x* and *y* coordinates) needs to be of high performance providing precise (step size of less than 0.5 μm is needed) translations in plane. Due to mechanical nature of the stage the data acquisition speed is lower. On the other hand, digital beam scan enables high speed data acquisition. The combination of both scanning modes offers possibility of large area scans with high speed. This is possible by employing stitching method on different scanned areas defined by stage coordinates, slightly overlapped with purpose to achieve seamless, as much as possible, composite image.

VIII. System calibration

In order to accurately index diffracted pattern, besides correctly defined crystal structure, the pattern must also be calibrated to the geometry of the EBSD system and a sample in SEM. Important part of calibration is to have accurately identified the pattern centre and distance between specimen and EBSD camera. The pattern centre is defined as the point of intersection on the EBSD camera and an electron beam perpendicular to both primary electron beam and the horizontal as shown in Fig. 8a.

From historical perspective, the early method was to use three suspended round balls and their elliptical shadows cast on the diffraction pattern [38]. In this approach the pattern centre was determined from long axes of elliptical shadows and their intersection on the pattern. Today more popular approach is to use a single crystal of known orientation and the most practical is a cleaved silicon crystal. The surface normal of the crystal should be [001] and the cleaved edge [110] parallel to the horizontal. Such arrangement makes certain that [114] crystal direction is normal to the EBSD camera and the location of the [114] zone axis identifies the pattern centre as shown in Fig. 8b. Based on this arrangement the [111] zone axis lies below the [114] zone axis and the vertical distance between [111] and [114] zone axes and angel between these directions are function of specimen to screen distance. Another calibration method involves translation of EBSD camera and collecting pattern at both working position and retracted position where the pattern centre is the only point to have the same location in both patterns.

IX. Sample preparation

Since EBSD patterns are collected from diffraction region within the top 50 nm of material the top surface region must be free from both contamination and residual deformation. If this condition is not satisfied the user will find that EBSD patterns are not visible and EBSD work impossible or barely visible and accuracy of EBSD work questionable. Surface contamination weakens and obscures diffracted EBSD patterns while deformation layer broadens EBSD patterns causing them to overlap and decreases sharpness of the patterns, which adversely affect accurate indexing. Only

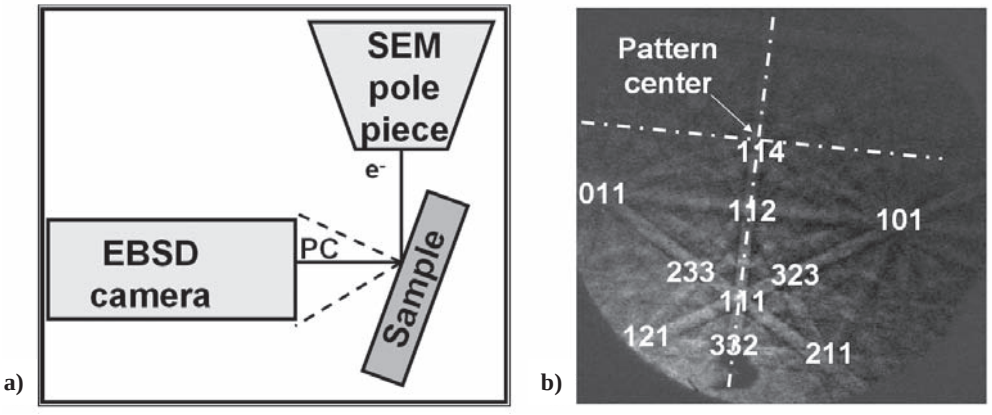

Figure 8. Diffraction pattern centre shown as a) schematic in SEM chamber, b) the location of the [114] zone axis in the diffraction pattern from silicon single crystal

proper sample preparation can produce contamination free and deformation free surface, the necessary conditions to obtain high quality EBSD patterns.

In general, a conventional metallographic sample preparation technique, comprised of sectioning, mounting, grinding and polishing, is a method of mechanical polishing and can produce a sample of limited quality for EBSD work. The following additional steps or techniques are necessary to obtain EBSD patterns of high quality.

Vibratory polishing subsequently applied after conventional metallographic technique for several minutes to several hours using solution of 0.02 μm colloidal silica. The solution polishes and slightly etches material, removing most of deformation layer on surface. It works well with almost any material, especially with ceramic and geological samples.

Electropolishing can also be applied after conventional metallographic technique for several seconds to several minutes in electrolytic solution where sample is made an anode. This method removes any remnant deformation layer and surface irregularities formed during mechanical polishing. There is no universal electrolytic solution that works with all materials and for given material it is necessary to identify right solution along with operating voltage, solution temperature, specimen size, the time of contact as well as the age of the solution (shelf life).

Chemical etching can be used as an alternative to electropolishing by emersion in chemical solution that selectively dissolves material on the surface. This method is effective in removing deformation layer on the surface due to the higher surface energy in deformation layer. For good results, it is also important to use proper solution and 5% nital solution (5% nitric acid and 95% ethanol by volume) is general solution that works well for many materials.

Ion etching is alternative for materials and samples (thin films, integrated circuits) that cannot be effectively prepared by listed techniques. During ion etching an ionized gas is accelerated toward the surface of the sample and during collision material from surface is removed. A caution needs to be exercised due to potential lattice damage in the sample during interaction with the high energy ions. In addition, an impact of high energy ions raises the temperature in material and the generated heat can alter the microstructure in material. For better results, it is recommended to use low voltage and low current for longer period of time. In addition, the advantage of high energy ions can be taken in removing of oxide films from specimen and cross-sectioning or serial-sectioning of specimen.

It is also very important that material of interest for study is conductive enough to avoid build up charge when exposed to an electron beam in SEM. Ceramic materials have high electrical resistivity (low conductivity) and require conductive coating to be placed on the surface of the sample in order to avoid EBSD pattern degradation and drifting of electron beam. Additional coating and its thickness decreases signal-to-noise ratio of the patter and carbon (with low atomic number) is used as the primary choice for coating material and thickness of up to 25 Å is recommended to provide adequate conductivity and still keep signal-to-noise ratio high. If indexing of diffracted patterns from the sample with coated surface becomes difficult the acceleration voltage on the SEM can be increased in order to increase beam penetration through applied coating.

In addition to published literature [39], recommended sample preparation procedures can also be found on respective websites of two manufacturers of EBSD equipment TSL/EDAX in USA [40] and HKL/Oxford Instruments in Europe [41] and respective websites of manufacturers of materialographic preparation equipment such as Buehler in USA [42] and Struers in Europe [43].

X. Applications

Over the last two decades an ample of research has been conducted using EBSD technique on various materials, initially carried at universities and research centers and lately in industry as well. Today, besides continuous increase in research activity by employing EBSD worldwide, the technique is also finding its way to complement other techniques and contributes to more detailed microstructure characterization and better understanding of material properties. Several such examples are presented below.

10.1 EBSD and nanoindentation

A sample of directionally solidified electrical steel (Fe with Si content of 3 wt.%) with columnar grain structure was deformed by plane strain compression to a true strain of 1.6 at room temperature with compression axis being parallel to the columnar axis of grains. After deformation, surface of compressed sample (perpendicular to compression axis) was prepared for EBSD study by conventional mechanical grinding and polishing, followed by final vibratory polishing (after vibratory polishing grain boundaries in a single phase alloy were clearly visible). After collected high-resolution EBSD map (Figs. 9a and 9c) the deformed sample was wrapped in stainless steel foil and partially annealed at 620 °C for 30 minutes in salt bath to obtain partially annealed structure (with recovered regions and recrystallized grains). After annealing, surface was repolished and new high-resolution EBSD map was obtained from the same location in order to identify and select individual recrystallized grains and well recovered but not recrystallized regions for nanoindentation using a spherical diamond tip with 13.5 μm radius (Figs. 9b and 9d). Figures 9a and 9b are Inverse Pole Figure (IPF) maps of the same area in deformed and partially annealed

state, respectively. In IPF maps each individual orientation of crystals is coloured differently and colour coding for orientations is presented in Standard Stereographic Triangle (SST), shown as inset in the bottom-right corner of the image. SST is a part of geometric mapping function that projects a sphere onto a plane and shows a segment of the sphere bounded by (001), (101) and (111) crystallographic poles, which spans all crystallographic orientations. Figure 9a reveals both primary grain boundaries and transition bands developed during deformation and Fig. 9b reveals preferentially formed recrystallized grains in the vicinity and along primary grain boundaries. Circled individual recrystallized grains and squared well recovered regions were selected for nanoindentation and study of stored energy (increase in dislocation density) after deformation and subsequent partial annealing. Figures 9c and 9d are grain boundary colour maps of the same area in deformed and partially annealed state, respectively. In grain boundary colour map different colours are assigned to different ranges of grain boundary misorientation, shown as inset in the bottom-right corner of the image. Grain boundaries with misorientation larger than 15 degree are considered high angle grain boundaries (HAGB) and are characterized as highly mobile grain boundaries. Figure 9c shows that primary grain boundaries are HAGB and that deformation bands in both top-left and bottom-left regions are also having HAGB character (coloured blue). It can be noticed that large fraction of low angle grain boundaries (LAGB) with misorientation less than 5 degree (coloured red) is present in deformed state due to increased dislocation density. Figure 9d shows that recrystallized grains have been primarily formed in the regions with large presence of HAGB after deformation. Two additional insets show magnified HAGB regions with formed recrystallized grains selected for nanoindentation. It can also be noticed that after partial annealing a fraction of HAGB has increased (from about 17% to 47%) mostly on behalf of decreased fraction of LAGB (from about 61% to 39%). From nanoindentation study it was concluded that dislocation density in recovered regions was by two orders of magnitude larger than in recrystallized grains. Demonstrated principles for characterization of crystallographic texture, grain boundary misorientation and dislocation density have been used to develop thermomechanical processing of electrical steel with preferred texture and optimum grain size [44].

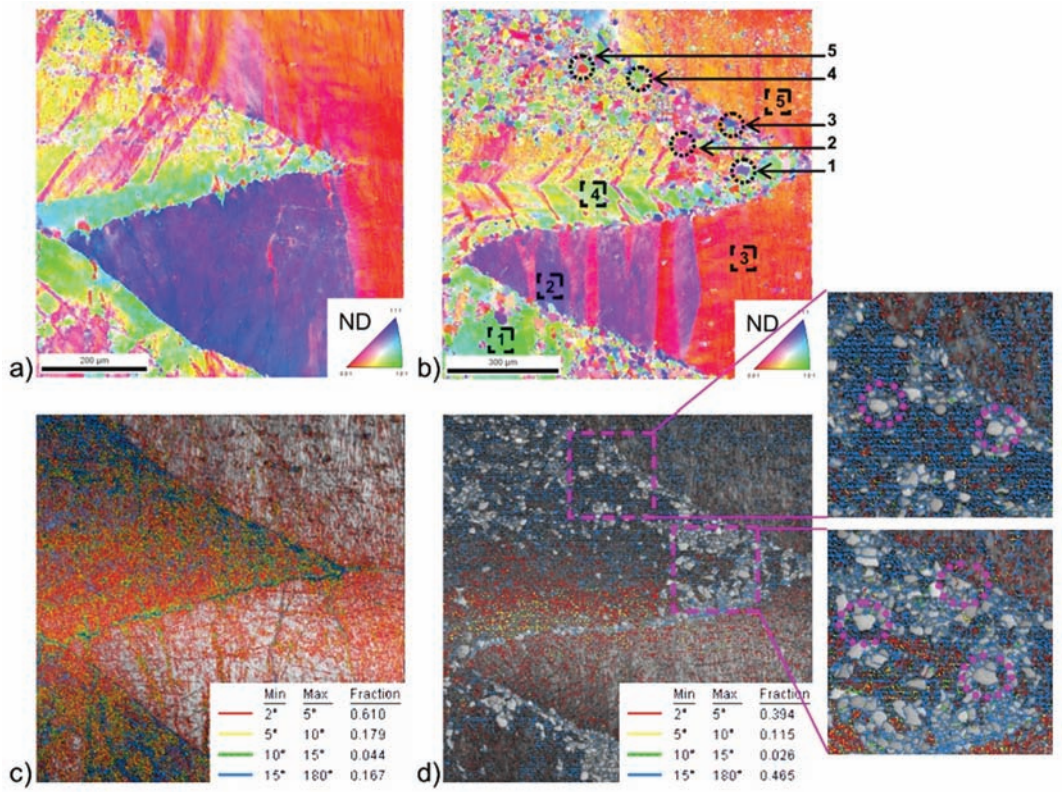

Figure 9. Inverse Pole Figure (IPF) maps in reference to normal (ND) direction of a) deformed sample, b) partially annealed sample (with selected recrystallized grains (circled) and well recovered regions (squared) for nanoindentation measurements) and grain boundary colour maps of c) deformed sample, d) partially annealed sample (with insets showing high angle boundaries (more than 15 degree are coloured blue) surrounding selected recrystallized grains) for nanoindentation study [35]. Characterization was carried out in FEI/Phillips XL 30 FEG ESEM equipped with TSL/EDAX Hikari EBSD detector and TSL OIM 5.1 software. Sample was tilted 70 degree with respect to the horizontal and data was collected at the acceleration voltage of 20 kV and working distance of 22 mm.

10.2 EBSD and energy dispersive spectroscopy

Combination of EBSD and Energy Dispersive Spectroscopy (EDS) improves the reliability of the phase differentiation in multiphase materials and has been used for characterization of inclusions in titanium alloy [45]. A sample of titanium alloy with multiple oxide inclusions was studied (Fig. 10). The image contains colour coded (different colour assigned to different phase) phase maps differentiated by conventional EBSD using crystallographic data only (Fig. 10a), by EDS using X-ray energy data for the major phases present, that are titanium and alumina (Figs. 10b and 10c, respectively), by combination of EBSD and EDS techniques (Fig. 10d). Disagreement in phase differentiation between EBSD and EDS (when used separately) is quite obvious (for some orientations in the large inclusions EBSD was not able to properly differentiate between titanium phase and alumina phase), but when EBSD and EDS are combined the phases are differentiated much more reliably including the minor phases present, which are identified as erbium oxide and monoclinic and tetragonal zirconium oxides. In addition to determination of the phases (location and volume fraction) within the microstructure, a known crystallographic relationship between different phases at the interface provides the more complete description of microstructure. EBSD can also be combined with Wavelength Dispersive Spectroscopy (WDS) [46]. Furthermore, with proper setup in the SEM all three techniques (EBSD, EDS and WDS) can be used simultaneously.

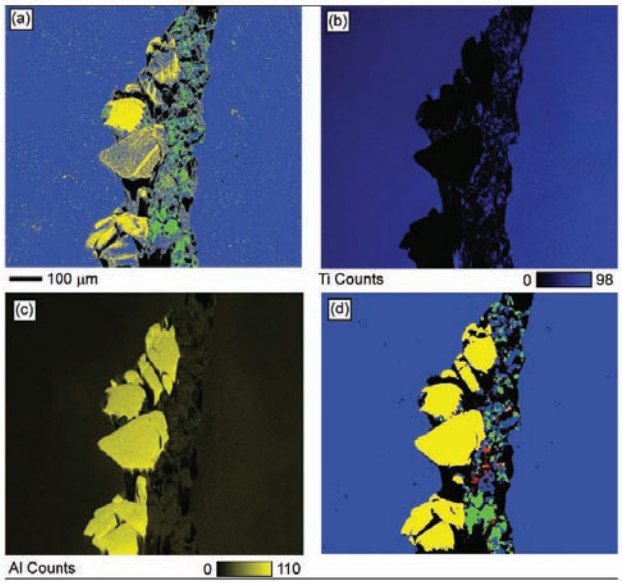

Figure 10. Phase maps for titanium alloy using a) conventional EBSD, b) titanium EDS, c) aluminium EDS and d) combined EBSD with the EDS filter. Phases are colour coded: blue for titanium, yellow for alumina, green for erbium oxide, red for monoclinic zirconium oxide and orange for tetragonal zirconium oxide [45]. With kind permission from John Wiley & Sons, Inc., *Journal of Microscopy*, "Phase differentiation via combined EBSD and XEDS", 213 [3] (2004) 296-305, M.M. Nowell, S.I. Right, Figure 6.

10.3 EBSD and atomic force microscopy

Atomic Force Microscopy (AFM), a high resolution technique, has been used in conjunction with EBSD to characterize segregation of rear earth elements at the grain boundary and its effect on thermal grooving [47]. Samples of fine grained undoped and ytterbium-doped alumina were studied (Fig. 11). It was found that addition of dopants to alumina has significantly increased the size of grain boundary grooves and AFM maps of surface topography show higher depth of thermal grooves along grain boundaries across mapped area (depth of grooves is colour coded by 150 nm colour bar on the right side of maps). EBSD data indicated that there is no correlation between segregation of rear earth elements at the grain boundary and grain boundary misorientation. Combined EBSD and AFM techniques were also used for study of anisotropy of tribological properties with respect to grain orientation. It was found that grain surfaces close to (0001) plane exhibited wear at higher rate. Effect of grain boundary segregation can be used for control of the grain size and improvement of sinterability, both of which improve mechanical properties of the material. Grain

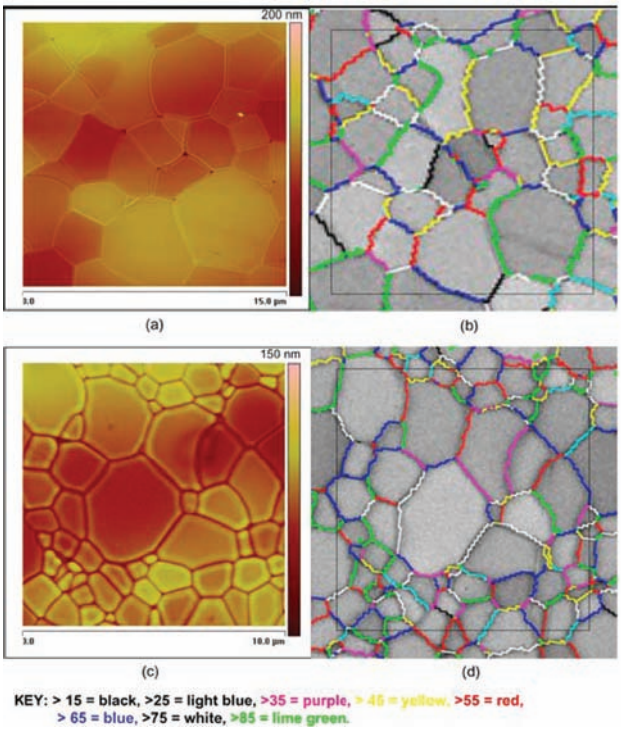

Figure 11. Atomic Force Microscopy (AFM) colour coded maps of surface topography (height) with nanometer scale bar on the right from a) undoped and c) ytterbium-doped alumina and corresponding EBSD grain boundary misorientation maps of b) undoped and d) ytterbium-doped alumina obtained from the same area, respectively, with shown below colour coded grain boundary misorientation values [47]. With kind permission from Springer Science + Business Media: *Journal of Materials Science*, "Characterization of fine-grained oxide ceramics", 39 (2004) 6687-6704, G.D. West, J.M. Perkins, M.H. Lewis, Figure 26.

boundary segregation can also have an adverse effect and increase susceptibility for grain boundary embrittlement and increased size of grain boundary grooves at elevated temperature can decrease fracture stress. In a different study, EBSD and AFM were used to investigate microstructural changes induced by irradiation in titanium-silicon-carbide and a result showed that irradiation induced swelling was anisotropic in studied material [48].

10.4 EBSD and focused ion beam

A Focused Ion Beam (FIB) in SEM enables collection of microstructure data from serial (parallel) sections which can be subsequently reconstructed into three-dimensional microstructure. For example, from only one prepared section for grain boundary study data is limited to the trace of grain boundary (intersecting line between grain boundary plane and examined surface) and angle between grain boundary plane and examined plane cannot be determined. For complete characterization of grain boundary character, information about grain boundary plane is needed and serial sectioning with proper alignment between sections allows for complete identification of grain boundary character, which is determined by the three lattice misorientation parameters (of two grains that share the same grain boundary) and the two grain boundary plane orientation parameters (relative to those two grains). A dual beam FIB-SEM system has been used for serial sectioning and collected EBSD data on triple junctions (a point where three grain boundary lines meet) from multiple sections has been used to define grain boundary planes and study grain boundary character [49]. Sample of fine grained undoped yttria was characterized and reconstructed three-dimensional microstructure is shown in Fig. 12. It was found that polycrystalline yttria has weak grain boundary anisotropy, which may result from the absence of closed packed planes in cubic structure of yttria. In another grain boundary character study the EBSD data was collected from magnesia sample with serial sections prepared by manual polishing which is a labor intensive process [50].

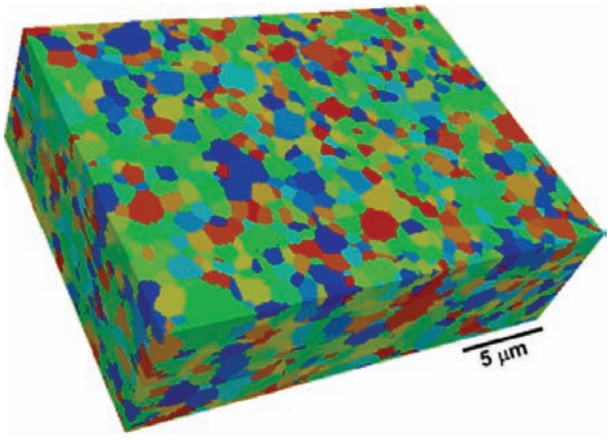

Figure 12. Reconstructed 43 collected and 280 nm spaced serial sections of EBSD data from undoped yttria [49]. With kind permission from John Wiley & Sons, Inc., *Journal of the American Ceramic Society*, "Characterization of the grain-boundary character and energy distributions of yttria using automated serial sectioning and EBSD in the FIB", 92 [7] (2009) 1580-1585, S.J. Dillon, G.S. Rohrer, Figure 3.

XI. Outlook

An automated EBSD has become a well established technique in materials characterization [51,52] and within the last several years the data acquisition rate has increased by an order of magnitude from several tens of data points per second to several hundred data points per second [53]. EBSD system with high speed data acquisition can be used for in-situ study of microstructure and texture evolution during deformation or annealing [54], phase transformations during heating and cooling [55], crack propagation during loading and unloading [56], domain switching in piezoelectric materials during loading and unloading [57]. With high speed data acquisition it is possible to collect, for example, one million data points within an hour. Collection of such large data sets can be treated as statistically meaningful and used for statistical description of microstructure (e.g. grain morphology, grain orientation and correlation between grains, grain misorientation and correlation between grains, grain boundary character distribution). Furthermore, statistical descriptors of microstructure [58] can extend their use in numerical models for simulations of microstructure evolution during processing [59].

Recently, it has been demonstrated that the high angular resolution analysis of EBSD patterns is possible by application of the 3D Hough transform and it has been shown that local stress analysis can be performed with high accuracy [60]. High level of accuracy should propel EBSD technique to be employed in the area of local stress and stress gradient measurements.

In recent years, EBSD has become a versatile characterization technique, thanks to advancement in both hardware and software developments. The other complementary techniques are making strides as well, especially in non-destructive 3D microstructure characterization with the emphasis on spatial resolution. A Three-Dimensional X-Ray Diffraction (3DXRD) microscopy has possibility of fast mapping of the microstructure at the scale of a few micrometers, which enables in-situ studies of the grains and subgrains during deformation, annealing and phase transformation [61]. Three-Dimensional Orientation Mapping in the TEM (3D-OMiTEM) was recently reported with a spatial resolution on the order of 1 nm, which is suitable for characterization of nanocrystalline thin film materials [62].

Nevertheless, EBSD has become a robust technique that plays a vital role in materials characterization and will continue to play an important role thanks to its versatility and compatibility with other techniques.

Acknowledgements: The author would like to thank Professor Emeritus Leposava Šiđanin and Professor Vladimir Srdić, both at the University of Novi Sad (Serbia), for suggestion and kind invitation to write on this topic. Author would also like to acknowledge that a portion of the research work presented in this paper and referenced in doctoral dissertation was made possible by support of the Centralized Research Facility at Drexel University (USA) and was funded by National Science Foundation (USA) under Division of Materials Research (DMR0303395).

References

1. S. Kikuchi, "Diffraction of cathode rays by mica", *Jpn. J. Phys.*, **5** (1928) 83–96.
2. S.I. Wright, *Ph.D. Thesis*, Yale University, USA 1992.
3. S. Nishikawa, S. Kikuchi, "The diffraction of cathode rays by calcite", *Proc. Imperial Acad. Jpn.*, **4** (1928) 475–477.
4. R. von Meibom, E. Rupp, "Wide angle electron diffraction", *Z. Physik*, **82** (1933) 690–696.
5. H. Boersch, "About bands in electron diffraction", *Physikalische Zeitschrift*, **38** (1937) 1000–1004.
6. K. Artmann, "On the theory of Kikuchi bands", *Z. Physik*, **125** (1948) 225–249.
7. M.N. Alam, M. Blackman, D.W. Pashley, "High-angle Kikuchi patterns", *Proc. Royal Society of London*, **A221** (1954) 224–242.
8. J.A. Venables, C.J. Harland, "Electron back-scattering patterns – A new technique for obtaining crystallographic information in the scanning electron microscope", *Philoso. Mag.*, **2** (1973) 1193–1200.
9. D.J. Dingley, "Diffraction from sub-micron areas using electron backscattering in a scanning electron microscope", *Scanning Electron Microsc.*, **11** (1984) 569–575.
10. Y. Inokuti, C. Maeda, Y. Ito, "Observation of generation of secondary nuclei in a grain oriented silicon steel sheet illustrated by computer color mapping", *J. Jpn. Inst. Metals*, **50** (1986) 874–878.
11. B.L. Adams, S.I. Wright, K. Kunze, "Orientation imaging: The emergence of a new microscopy", *Met. Trans.*, **24A** (1993) 819–831.
12. D.J. Dingley, K. Baba-Kishi, "Use of Electron Backscatter Diffraction Patterns for determination of crystal symmetry elements", *Scanning Electron Microsc.*, **11** (1986) 383–391.
13. D.J. Dingley, R. Mackenzie, K. Baba-Kishi, "Application of backscatter Kikuchi diffraction for phase identification and crystal orientation measurements in materials", pp. 435–436 in *Microbeam Analysis*. Ed. P.E. Russell, San Francisco Press, 1989.
14. D.J. Dingley, M. Longdon, J. Wienbren, J. Alderman, "On-line analysis of electron backscatter diffraction patterns, texture analysis of polysilicon", *Scanning Electron Microsc.*, **11** (1987) 451–456.
15. N.-H. Schmidt, N.Ø. Olesen, "Computer-aided determination of crystal-lattice orientation from electron-channeling patterns in the SEM", *Can. Mineral.*, **27** (1989) 15–22.
16. D. Juul-Jensen, N.H. Schmidt, "Automatic recognition of electron backscattering patterns", pp. 219–224 in *Proceedings of Recrystallization '90*. Ed. by T.C. Chandra, TMS, Warrendale, Pennsylvania, 1990.
17. S.I. Wright, B.L. Adams, J.-Z. Zhao, "Automated determination of lattice orientation from electron backscattered Kikuchi diffraction patterns", *Textures Microstruct.*, **13** (1991) 123–131.
18. S.I. Wright, B.L. Adams, "Automatic analysis of electron backscatter diffraction patterns", *Met. Trans. A*, **23** (1992) 759–767.
19. J.C. Russ, D.S. Bright, J.C. Russ, T.M. Hare, "Application of the Hough transform to electron diffraction patterns", *J. Computer-Assisted Microsc.*, **1** (1989) 3–37.
20. N.C. Krieger-Lassen, K. Conradsen, D. Juul-Jensen, "Image processing procedures for analysis of electron back scattering patterns", *Scanning Microsc.*, **6** (1992) 115–121.
21. K. Kunze, S.I. Wright, B.L. Adams, D.J. Dingley, "Advances in automatic EBSP single orientation measurements", *Textures Microstruct.*, **20** (1993) 41–54.
22. D.P. Field, "Recent advances in the application of orientation imaging", *Ultramicrosc.*, **67** (1997) 1–9.
23. S.I. Wright, D.P. Field, "Analysis of multiphase materials using electron backscatter diffraction", pp. 561–562 in *Proc. Microscopy and Microanalysis '97*. Eds. G.W. Bailey, R.V.W. Dimlich, K.B. Alexander, J.J. McCarthy, T.P. Pretlow, Springer, 1997.
24. S.I. Wright, M.M. Nowell, "Chemistry assisted phase differentiation in automated electron backscatter diffraction", pp. 682CD in *Proceedings Microscopy and Microanalysis 2002*, Québec City, Québec, Canada, Cambridge University Press, 2002.
25. H.C. Sorby, "On the microsopical structure of iron and steel", *J. Iron Steel Inst.*, **1** (1887) 255–288.
26. R. Castaing, *Ph.D. Thesis*, University of Paris, France, 1951.
27. H.J. Bunge, *Texture analysis in materials science. Mathematical Methods*, Cuvillier Verlag, Göttingen, 1993.
28. J.F. Nye, *Physical Properties of Crystals*, Oxford University Press, Oxford, 1969.
29. W.H. Bragg, W.L. Bragg, *X rays and Crystal Structure*, G. Bell and Sons Ltd, London, 1915.
30. P.V.C. Hough, "Machine analysis of bubble chamber pictures", pp. 554–556 in *Proc. Int. Conf. High Energy Accelerators and Instrumentation*, CERN, Geneva, Switzerland, 1959.
31. R.O. Duda, P.E. Hart, "Use of the Hough transformation to detect lines and curves in pictures", *Comm. ACM*, **15** (1972) 11–15.

32. W.H. Miller, *A Treatise on Crystallography*, Cambridge: for J. & J.J. Deighton and London: for John W. Parker 1839.
33. P.M. Jones, G.M. Rackham, J.W. Steeds, "Higher order Laue zone effects in electron diffraction and their use in lattice parameter determination", *Proc. Roy. Soc. London*, **A 354** (1977) 197–222.
34. S. Wright, M. Nowell, "EBSD image quality mapping", *Microsc. Microanal.*, **12** (2006) 72–84.
35. A.J. Wilkinson, D.J. Dingley, "Quantitative deformation studies using electron backscatter patterns", *Acta Metall. Mater.*, **39** [12] (1991) 3047–3055.
36. D. Stojakovic, *Ph.D. Thesis*, Drexel University, USA 2008.
37. K.Z. Troost, "Towards submicron crystallography in the SEM" *Philips J. Res.*, **41** (1993) 151–163.
38. J.A. Venables, R. Bin-Jaya, "Accurate microcrystallography using electron back-scattering patterns", *Philos. Mag.*, **35** (1977) 1317–1328.
39. M.M. Nowell, R.A. Witt, B. True, "EBSD sample preparation: Techniques, tips and tricks", *Microsc. Microanal.*, **11** (2005) 504–505.
40. www.edax.com
41. www.ebsd.com
42. www.buehler.com
43. www.struers.com
44. D. Stojakovic, R.D. Doherty, S.R. Kalidindi, F.J. G. Landgrad, "Thermomechanical processing for recovery of desired <001> fiber texture in electric motor steels", *Metall. Mater. Trans. A*, **39A** (2008) 1738–1746.
45. M.M. Nowell, S.I. Wright, "Phase differentiation via combined EBSD and XEDS", *J. Microsc.*, **213** [3] (2004) 296–305.
46. M. Faryna, K. Sztwiertnia, K. Sikorski, "Simultaneous WDXS and EBSD investigations of dense PLZT ceramics", *J. Eur. Ceram. Soc.*, **26** [14] (2006) 2967–2971.
47. G.D. West, J.M. Perkins, M.H. Lewis, "Characterization of fine-grained oxide ceramics", *J. Mater. Sci.*, **39** (2004) 6687–6704.
48. J.C. Nappé, C. Maurice, Ph. Grosseau, F. Audubert, L. Thomé, B. Guilhot, M. Beauvy, M. Benabdesselam, "Microstructural changes induced by low energy heavy ion irradiation in titanium silicon carbide", *J. Eur. Ceram. Soc.*, **31** [8] (2011) 1503–1511.
49. S.J. Dillon, G.S. Rohrer, "Characterization of the grain-boundary character and energy distribution of yttria using automated serial sectioning and EBSD in the FIB", *J. Am. Ceram. Soc.*, **92** [7] (2009) 1580–1585.
50. D.M. Saylor, A. Morawiec, G.S. Rohrer, "The relative free energies of grain boundaries in magnesia as a function of five macroscopic parameters", *Acta Mater.*, **51** [13] (2003) 3675–3686.
51. O. Engler, V. Randle, *Introduction to Texture Analysis: Macrotexture, Microtexture and Orientation Mapping – 2nd ed.*, CRC Press by Taylor and Francis Group, Boca Raton, 2010.
52. A.J. Schwartz, M. Kumar, B.L. Adamas, D.P. Field, *Electron Backscatter Diffraction in Materials Science – 2nd ed.*, Springer Science and Business Media, New York 2009.
53. M.M. Nowell, M. Chui-Sabourin, J.O. Carpenter, "Recent advances in high-speed orientation mapping", *Microsc. Today*, **14** [6] (2006) 6–9.
54. D.P. Field, L.T. Bradford, M.M. Nowell, T.M. Lillo, "The role of annealing twins during recystallization of Cu", *Acta Mater.*, **55** (2007) 4233–4241.
55. I. Lischewski, D.M. Kirch, A. Ziemons, G. Gottstein, "Investigation of the α-γ-α transformation in steel: High temperature in situ EBSD measurements", *Texture, Stress and Microstructure*, **2008** (2008) 1–7.
56. S. Ifergane, Z. Barkay, O. Beeri, N. Eliaz, "Study of fracture evolution in copper sheets by in situ tensile test and EBSD analysis", *J. Mater. Sci.*, **45** (2010) 6345–6352.
57. M. Karlsen, M-A. Einarsrud, H.L. Lein, T. Grande, J. Hjelen, "Backscatter electron imaging and electron backscatter diffraction characterization of $LaCoO_3$ during in situ compression", *J. Am. Ceram. Soc.*, **92** [3] (2009) 732–737.
58. S. Torquato, "Statistical description of microstructures", *Annu. Rev. Mater. Res.*, **32** (2002) 77–111.
59. D.T. Fullwood, S.N. Niezgoda, B.L. Adams, S.R. Kalidindi, "Microstructure sensitive design for performance optimization", *Prog. Mater. Sci.*, **55** [6] (2010) 477–562.
60. C. Maurice, R. Fortunier, "A 3D Hough transform for indexing EBSD and Kossel patterns", *J. Microsc.*, **230** [3] (2008) 520–529.
61. D. Juul Jensen, E.M. Lauridsen, L. Margulies, H.F. Poulsen, S. Schmidt, H.O. Sørensen, G.B.M. Vaughan, "X-ray microscopy in four dimensions", *Mater. Today*, **9** [1-2] (2006) 18–25.
62. H.H. Liu, S. Schmidt, H.F. Poulsen, A. Godfrey, Z.Q. Liu, J.A. Sharon, X. Huang, "Three-dimensional orientation mapping in the transmission electron microscope", *Science*, **332** (2011) 833–834.